Acta Cryst. (1988). B44, 362–367

Electron-Density Distribution in Magnesite ($MgCO_3$)

BY S. GÖTTLICHER AND A. VEGAS*

Institut für Physikalische Chemie, Fachgebiet Strukturforschung, Technische Hochschule, Petersenstrasse 20, D-6100 Darmstadt, Federal Republic of Germany

(*Received* 3 *June* 1987; *accepted* 26 *February* 1988)

Abstract

The electron-density distribution in natural magnesite, $MgCO_3$, has been determined from absolute X-ray diffraction data measured on single-crystal plates. Crystal data are $M_r = 84{\cdot}3$, $R\bar{3}c$, $a = 4{\cdot}636$ (1), $c = 15{\cdot}026$ (2) Å, $V = 279{\cdot}6$ (1) Å^3, $Z = 6$, $D_x = 3{\cdot}0$ Mg m^{-3}, experimental μ(Mo $K\alpha$) = 0·564 mm^{-1}, λ(Mo $K\alpha_1$) = 0·7070 Å, $F(000) = 252$. Conventional refinement to $R = 0{\cdot}025$ from 300 reflections up to $(\sin\theta)/\lambda = 1{\cdot}0$ Å^{-1} was made. Anisotropic primary-extinction correction [Zachariasen (1967). *Acta Cryst.* **23**, 558–564] was applied. The deformation maps show maxima of 0·50 e Å^{-3} in the C—O bond and in regions of the O-atom lone pairs, and no disorder is observed in the planar CO_3^{2-} anions. In the absolute-density maps, ρ has minima of 2·55 e Å^{-3} at the midpoint of the C—O bond and of 0·18 e Å^{-3} between the Mg and O atoms, which was interpreted as an ionic interaction between Mg^{2+} and CO_3^{2-} ions. The spherical integration of ρ around the Mg atom gives 10·10 e; however, an overlap density $\rho = 0{\cdot}24$ e Å^{-3} is found between the two O atoms forming the longest distance (3·020 Å) of the MgO_6 octahedron.

Introduction

Electron-density studies have received much attention in the last years. Most of them have dealt with deformation-density maps obtained either from a combination of relative X-ray and neutron diffraction data, the so-called $X-N$ maps, or from X-ray diffraction data only. In the latter case, positional and thermal parameters are obtained from the high-order reflections and the $\Delta\rho$ maps are known as $X-X$ maps. On the other hand, studies aimed at the determination of electron density on an absolute scale are scarce. Of them, those of Mg_2Si (Panke & Wölfel, 1969), LiOH (Göttlicher & Kieselbach, 1976) and $NaNO_3$ (Göttlicher & Knöchel, 1980) are the most recently reported.

For calcite-like compounds, such as $NaNO_3$, the space-group symmetry requires planar XO_3 groups although deviation from planarity was suggested. So the IR spectrum of $NaNO_3$ could only be interpreted on the assumption of a pyramidal model for the NO_3^- ion (Schäfer, Matosi & Aderhold, 1930) which was also proposed by Pauling (1931) on the basis of quantum-mechanical calculations. This was confirmed by electron-density maps (Göttlicher & Knöchel, 1980) which showed the nitrate anions as flat pyramids with a height of 0·1 Å and slightly rotated from their special position, but arranged statistically so that the space group $R\bar{3}c$ holds for the whole crystal.

Distortions of the XO_3 groups also occur in many other compounds. Exhaustive studies have recently been reported for orthoborates (Zobetz, 1982) and for carbonates (Zemann, 1981).

Disorder of the CO_3^{2-} anion in calcite and magnesite was also suggested by several authors. So in a preliminary communication on the electron density of calcite (Peterson, Ross, Gibbs, Chiari, Gupta & Tossell, 1979), the rigid-body analysis of the CO_3 group was considered to be consistent with positional disorder which was interpreted as a screw motion parallel to **c**. Similar results were obtained for calcite in a high-temperature refinement of calcite and magnesite (Markgraf & Reder, 1985). However, the structure refinement of calcite, with data at 1073 K, could be made in the space group $R\bar{3}c$ and the Fourier maps showed no extra peaks due to positional disorder of the O atoms. For magnesite, orientational disorder was also suggested (Burton & Kikuchi, 1984) to explain the poor fit between experimental and calculated phase diagrams, although neither disorder nor distortion have been discussed in two previous X-ray structure refinements (Oh, Morikawa, Iwai & Aoki, 1973; Effenberger, Mereiter & Zemann, 1981). Finally, in an electron-density study of dolomite, $CaMg(CO_3)_2$, based on X-ray and neutron data, the CO_3^{2-} anions appear pyramidally distorted with the C atom shifted by 0·018 (1) Å from the O_3 plane (Effenberger, Kirfel & Will, 1983).

A second interesting aspect refers to the nature of the Mg—O bond. In the work on dolomite cited above, positive regions in the difference Fourier syntheses were observed at the midpoints of the Ca—O and Mg—O lines, suggesting the covalency of both bonds. Similar conclusions were deduced for the Mg—O bond from a comparative study of electron-charge distribution in

* Permanent address: Instituto de Química Inorgánica 'Elhúyar', CSIC, Serrano 113, 28006 Madrid, Spain.

0108-7681/88/040362-06$03.00

*M*O (*M* = Mg, Ca, Sr, Ba) oxides (Vidal-Valat, Vidal & Kurki-Suonio, 1978). On the other hand, a fully ionic character has been assigned to MgO from LCAO calculations (Causa, Dovesi, Pisani & Roetti, 1986).

We have undertaken the present study on $MgCO_3$ to determine the geometry and the bonds in the carbonate group and the type of bond between O and Mg atoms.

Experimental

(*a*) *Crystal preparation and intensity measurements*

Unit-cell parameters were obtained by least-squares refinement of the 2θ values determined on a powder sample, using Co $K\alpha$ radiation. The values agree with those reported for synthetic magnesite (Oh, Morikawa, Iwai & Aoki, 1973).

Two bulky crystals of natural magnesite ($MgCO_3$) were ground parallel to (100) and (110), respectively, resulting in two plates of approximate sections 1·5 × 1·0 cm. These two plates were used to measure the intensities of 3680 reflections, most of them in the symmetrical transmission setting on an automated four-circle diffractometer. The remaining reflections were measured in asymmetrical transmission but always minimizing the angle between the incident beam and the normal to the crystal plane. Measurements were carried out up to $(\sin\theta)/\lambda = 1{\cdot}0$ Å^{-1}, at plate thickness t = 1·89, 1·59, 0·98 and 0·44 mm for the (100) plate and t = 1·55, 1·20, 0·91 and 0·32 mm for the (110) plate, using LiF-monochromated and further-collimated (0·8 × 0·8 mm) Mo $K\alpha_1$ radiation. The ω-scan mode was used, with a scan width $\omega = \theta \pm 2{\cdot}5°$, at a speed of 0·2° min^{-1}. Background was measured at both ends of the scan range over 10 min, the total measuring time per reflection being 45 min. The detector apertures were 12 × 12 mm and the crystal-to-detector distance was 172 mm (equivalent aperture of 4° × 4°).

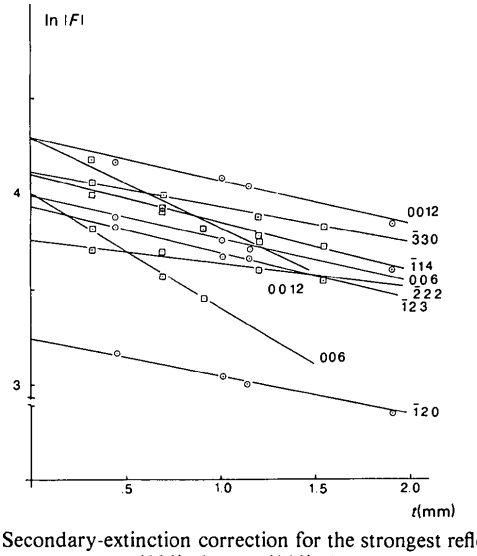

Fig. 1. Secondary-extinction correction for the strongest reflections. ⊙ (100) plate, ⊡ (110) plate.

Direct-beam intensity measurements were made every 8 h using a glass filter with an attenuation factor of 70·5. This attenuation filter was also used to measure the strongest reflections whose maxima were out of the linear region of the scintillation counter.

The moduli $|F_{hkl}|$ were calculated after correction for background, Lorentz and polarization factors and absorption effects as previously reported for NaCl (Göttlicher, 1968).

A secondary-extinction correction was applied to all reflections for which variation in the $|F|$ values with thickness t was observed. Their absolute moduli were determined by plotting $\ln|F|$ *versus* t and extrapolation to $t = 0$ (Fig. 1). For the weak reflections without secondary extinction this procedure was only an averaging of the structure factors. The accuracy of the results has been improved and double reflection has been detected and corrected.

Attempts were made to determine the absolute intensity for several strong reflections from powder samples but significant differences were observed between the intensities measured in transmission and reflection settings, indicating that, besides other factors, texture effects were present.

(*b*) *Primary-extinction correction*

A first least-squares refinement was carried out with the high-order data [$(\sin\theta)/\lambda > 0{\cdot}7$ Å^{-1}] starting with the parameters reported by Oh, Morikawa, Iwai & Aoki (1973). This resulted in an unexpectedly poor fit ($R = 0{\cdot}046$) with significant ΔF values for some strong high-order reflections. Further structure-factor calculations with the complete data set also showed ΔF's up to 30% for all strong extinction-corrected reflections. It was therefore assumed that primary extinction may be present, as occurred in the Mg_2Si crystals (Panke & Wölfel, 1969). A correction for this effect was tried applying the theory of Zachariasen (1967), in which the extinction factor, defined as $y = P/P_{kin}$, can be written as $y = (1 + 2x)^{-1/2}$, where x depends on the crystallite shapes.

In our case, two models were applied: that of spheres of radius r and that of plates of thickness D_0 in the symmetrical Laue case (Zachariasen, 1967). For the former, x can be written as

$$x_R = 3\left|\frac{e^2 Fk\lambda r}{mc^2 V}\right|^2 \Big/ 2\sin 2\theta \qquad (1)$$

$$k^2 = 1/2(1 + \cos^2 2\theta)$$

and for the latter

$$x_T = \left|\frac{e^2 Fk\lambda D_0}{mc^2 V}\right|^2 \Big/ 3\cos^2\theta. \qquad (2)$$

The spherical model was first applied. From the plot of I_o/I_c *versus* I_c, we obtained a value of $r = 12{\cdot}25$ μm which with (1) gave the value of x from which the extinction factor y was calculated and used to correct all the intensities. The results are represented in Fig. 2 where it can be seen that the I_o/I_c values of the $00l$ reflections do not fit the curve describing this model.

Moreover, the least-squares refinement and the subsequent valence Fourier maps, computed as explained later, were not satisfactory as indicated by some regions of negative electron density ($\rho = -0{\cdot}5$ e Å^{-3} at 0·29, 0, 0; $\rho = -0{\cdot}33$ e Å^{-3} at 0·30, 0·30, 0·25 and $\rho = -0{\cdot}25$ e Å^{-3} at 0·20, 0·38, 0).

This led us to consider the anisotropy in the crystallite shape by applying the second extinction model to the $00l$ reflections. A value of $D_0 = 28$ μm was obtained for the plate thickness.

So the final extinction parameter is given by the expression

$$y = (1 + 2x_R)^{-1/2}[g_r + \{1 - (lc^*)^2 \times [(h^2 + k^2 + hk)a^{*2} + l^2c^{*2}]^{-1}\}(1 - g_r)] + (1 + 2x_T)^{-1/2}\{(1 - g_r)(lc^*)^2 \times [(h^2 + k^2 + hk)a^{*2} + l^2c^{*2}]^{-1}\}, \quad (3)$$

where x_T and x_R are defined in (1) and (2) and g_r is a factor which accounts for the ratio between the two models. For $g_r = 1$, only the spherical model is taken into account; for $g_r = 0$, the calculation is made on the basis of both models but with values which vary with reciprocal-space directions. So, for $hk0$ reflections, the second term becomes zero and the extinction factor is that obtained for the spherical model; for $00l$ reflections, however, the spherical term of (3) vanishes and only the symmetrical Laue case is taken into account. In all the calculations g_r was set to 0.

Fourier maps showed a significant negative region at 0·29, 0, 0 of $-0{\cdot}20$ e Å^{-3}. This value decreased to $\rho = -0{\cdot}15$ e Å^{-3} by changing the sign of the weak reflection 431 (final $F_o = -2{\cdot}17$). After further small corrections on ten strong reflections the final minimal $\Delta\rho$ became $-0{\cdot}08$ e Å^{-3}.

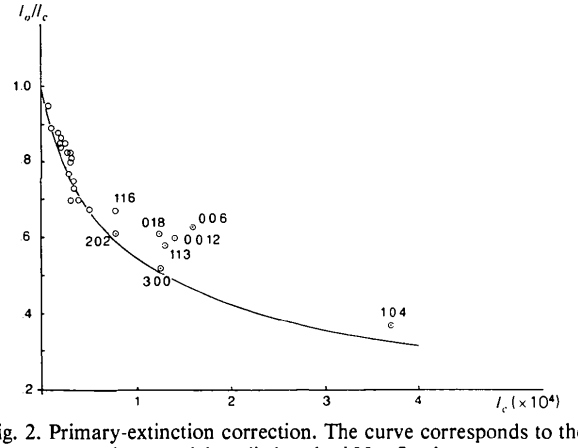

Fig. 2. Primary-extinction correction. The curve corresponds to the sphere model applied to the $h00$ reflections.

A final correction for TDS was applied as described previously (Göttlicher & Knöchel, 1980). Its contribution to the intensities was calculated from the elastic constants reported by Humbert & Plique (1972). TDS contributions have been calculated for 100 reflections with different magnitudes and directions of the scattering vectors. The result was an isotropic increase of the dB values in the temperature factor between 0·0925 and 0·0935 according to the formula

$$|F_o|_{corr} = |F_o| \exp[-dB\ (\sin^2\theta)/\lambda^2].$$

Therefore all structure factors have been multiplied by $\exp[-0{\cdot}093\ (\sin^2\theta)/\lambda^2]$.

Least-squares refinement and difference Fourier syntheses

With the structure factors corrected for the effects just described, a first anisotropic refinement (on F) was carried out. All 300 reflections were considered observed and unit weight was assigned to every reflection. Atomic scattering factors for Mg^{2+}, O and C were taken from *International Tables for X-ray Crystallography* (1974). After two cycles, with the scale factor fixed at 1·0, the refinement converged to $R = \sum||F_o| - |F_c||/\sum|F_o| = 0{\cdot}025$, the fit was good to 0·5865 and the maximal correlation factor was $-0{\cdot}3845$ for variables 3 and 4 (β_{11} and β_{33} of the C atom). A further cycle was made in which the scale factor was allowed to vary and a value of 0·997 was obtained without any difference in the atomic parameters (Table 1*). The ΔF synthesis is represented in Fig. 3 which corresponds to sections $xy\frac{1}{4}$ and $x0z$. Maximum shift/e.s.d. in last cycle = 0·03.

Calculation of the absolute electron density

The method consists of separating the electron density into two parts

$$\rho = \rho_1 + \rho_2. \quad (4)$$

ρ_1 is the contribution of the core electrons for which a spherical distribution is assumed and which can be obtained by means of Fourier integrals calculated at the atomic positions and referred to the principal ellipsoid axes. The non-spherical part ρ_2 is obtained by difference Fourier series. Consequently, the total density ρ is free of termination errors of the series.

* A list of observed and calculated structure factors has been deposited with the British Library Document Supply Centre as Supplementary Publication No. SUP 44797 (2 pp.). Copies may be obtained through The Executive Secretary, International Union of Crystallography, 5 Abbey Square, Chester CH1 2HU, England.

Table 1. *Atomic positional and thermal* ($\times 10^3$) *parameters for* $MgCO_3$

The temperature factor has the expression $T = \exp-(\beta_{11}h^2 + \beta_{22}k^2 + \ldots + 2\beta_{13}hl + 2\beta_{23}kl)$ or $T = \exp-[U_{11}(ha^*)^2 + U_{22}(kb^*)^2 + \ldots 2U_{13}hla^*c^* + \ldots]$. E.s.d.'s are given in parentheses.

	x	y	z	β_{11}	β_{22}	β_{33}	β_{12}	β_{13}	β_{23}
Mg	0	0	0	7·99(14)	7·99(14)	0·53(1)	4·00(7)	0	0
C	0	0	$\frac{1}{4}$	7·86(30)	7·86(30)	0·43(3)	3·93(15)	0	0
O	0·2775(1)	0	$\frac{1}{4}$	7·28(16)	10·02(25)	0·77(2)	5·01(12)	−0·16(3)	−0·32(6)

	U_{11}	U_{22}	U_{33}	U_{12}	U_{13}	U_{23}
Mg	6·52 (11)	6·52 (11)	6·06 (11)	3·26 (5)	0	0
C	6·42 (24)	6·42 (24)	4·91 (34)	3·21 (12)	0	0
O	5·94 (12)	8·18 (28)	8·80 (23)	4·09 (10)	−0·49 (9)	−0·98 (18)

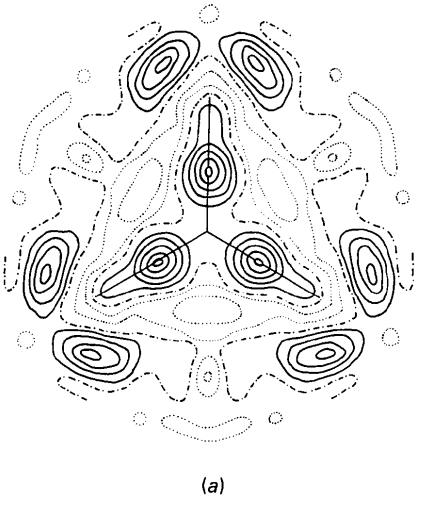

(*a*)

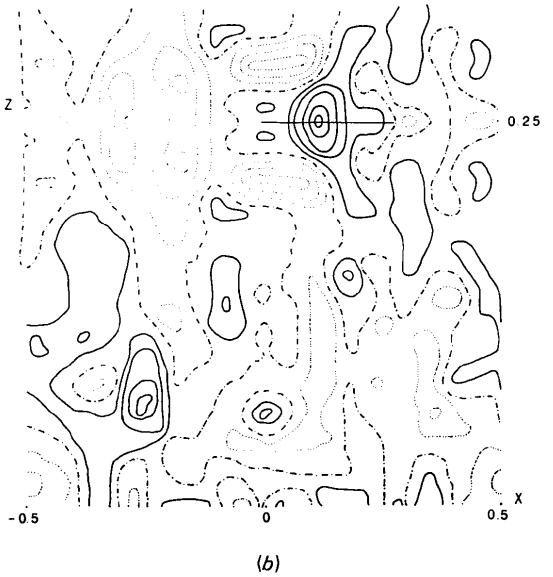

(*b*)

Fig. 3. Deformation density ($\rho_o - \rho_c$) in $MgCO_3$. (*a*) Section $xy\frac{1}{4}$ showing the plane of the CO_3^{2-} anion. (*b*) Section $x0z$ showing the residual charge at the C–O bond, perpendicular to the CO_3 plane. Contours are drawn at intervals of 0·1 e Å^{-3}. Zero lines are dot-dashed and dotted lines correspond to negative values.

Table 2. *Parameters of the Gaussian functions fitted to the theoretical atomic scattering factors*

	A_1(e atom^{-1})	a_1(Å^2)	A_2(e atom^{-1})	a_2(Å^2)
Mg	1·2197	0·1238	5·7982	2·5760
C	1·1293	0·2921	0·6625	1·1875
O	1·6659	0·2400	1·9946	5·0000

Table 3. *Atomic parameters for* $MgCO_3$ *after refinement with high-order data and Gaussian terms*

	Population parameter	x	y	z
Mg	0·1691 (19)	0	0	0
C	0·1713 (42)	0	0	$\frac{1}{4}$
O	0·5090 (59)	0·27708 (9)	0	$\frac{1}{4}$

	β_{11}	β_{22}	β_{33}	β_{12}	β_{13}	β_{23}
Mg	3·42 (25)	3·42 (25)	0·25 (2)	1·71 (12)	0	0
C	6·77 (51)	6·77 (51)	0·46 (4)	3·38 (26)	0	0
O	6·74 (24)	9·24 (27)	0·76 (2)	4·62 (13)	−0·18 (1)	−0·36 (2)

The calculation was made in the following steps:

(1) The atomic scattering factors at $(\sin\theta)/\lambda > 0{\cdot}7$ Å^{-1} are approximated to Gaussian functions of the form

$$f_1 = \sum_j A_j \exp[-a_j(\sin^2\theta)/\lambda^2]. \quad (5)$$

In our case, approximation was achieved for $j = 2$ and their values are listed in Table 2.

(2) These Gaussian coefficients and exponents are fitted to the experimental data, in the same range of $\sin\theta$, by means of a least-squares refinement in which the population parameters are allowed to vary together with the anisotropic thermal parameters. Thus, the new scattering factors can be expressed as

$$f_2 = \sum_j A'_j \exp\left(-\sum_i^3 \sum_k^3 \beta_{ik} h_i h_k\right). \quad (6)$$

Such a refinement for $MgCO_3$ converged after two cycles up to $R = 0{\cdot}022$ and led to the parameters quoted in Table 3.

(3) With these parameters, structure factors were calculated for all data and a ΔF synthesis was computed to obtain the non-spherical electron density ρ_2.

(4) Determination of the principal axes of the ellipsoids (Waser, 1955) and Fourier transform of the Gaussians to obtain ρ_1 for each atom. The expression used is

$$\rho_1(x,y,z) = \sum_i A'_i(\pi^3/e_{i1}e_{i2}e_{i3})^{1/2} \times \exp\{-\pi^2(x^2/e_{i1} + y^2/e_{i2} + z^2/e_{i3})\}, \quad (7)$$

where $e_{ij} = 1/4a_i + \lambda_j$ and x, y, z are the Cartesian coordinates with the origin at the nuclear position of each atom, λ_j being the square of the length of the principal axes of the thermal ellipsoids.

(5) Addition of $\rho_1 + \rho_2$ leads to the absolute electron density ρ. Two sections of ρ are represented in Figs. 4 and 5.

Discussion

From the deformation-density map (see Figs. 3*a* and 3*b*), neither deviation from planarity nor disorder were observed in the CO_3 group. At the nuclear positions, values of $\Delta\rho < 0{\cdot}08$ e Å^{-3} were found. A maximum of $0{\cdot}50$ e Å^{-3} appears at the midpoint of the C–O bond and two other maxima of $0{\cdot}52$ e Å^{-3}, related by a twofold axis, are observed in the lone-pair region of the O atom, forming with it an angle of 101 (1)°. One of these maxima is centred at 0·40, 0·09, 0·235, out of the CO_3 plane and directed towards the Mg atom although shifted from the Mg–O bond line, the distance to the Mg and O atoms being 1·90 (5) and 0·55 (5) Å, respectively. Another symmetry-related lone-pair maximum can be observed in the lower left side of Fig. 3*b*, near the Mg atom at the origin. In the same figure, it can be also observed that the maximum at the C–O bond is elongated in the *c* direction as a consequence of the π bonding between the two atoms.

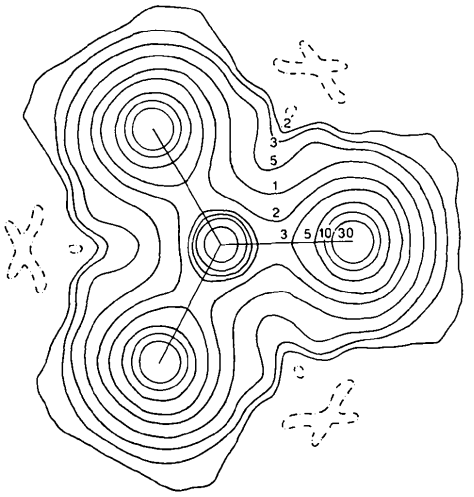

Fig. 4. Absolute electron density (e Å^{-3}) in $MgCO_3$. Section $xy\frac{1}{4}$ corresponding to the CO_3^{2-} anion.

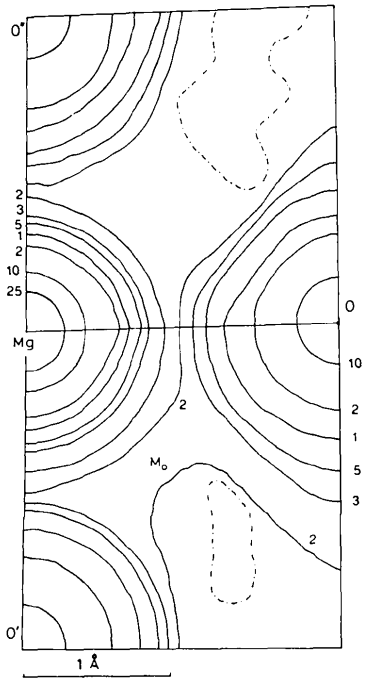

Fig. 5. Absolute electron density (e Å^{-3}) in $MgCO_3$ of the equatorial plane of an MgO_6 octahedron showing the electron bridge (M_O) between two O atoms. Only one half has been represented, the other half being equivalent through a centre of symmetry at the Mg position.

Similar results were reported for the CO_3^{2-} anion in dolomite, $CaMg(CO_3)_2$ (Effenberger, Kirfel & Will, 1983); however, the maxima in the lone-pair region are more clearly defined in our study.

The important question of the nature of the Mg–O bond cannot be elucidated from the existence of these maxima but only with the absolute-electron-density maps represented in Figs. 4 and 5 which will be discussed below.

The absolute ρ values at the nuclear positions are 101·6, 119·0 and 331·4 e Å^{-3} for C, O and Mg, respectively. These values are not significant and depend on the thermal vibrations. Along the C–O bond (see Fig. 4) there is a minimum of $\rho = 2{\cdot}55$ e Å^{-3} at $x = 0{\cdot}11$ just between the 3 e Å^{-3} curves. This value is somewhat lower than that of 2·9 e Å^{-3} reported for the absolute electron density in the N–O bond (Göttlicher & Knöchel, 1980).

In contrast, in the difference-density map the residual value in $MgCO_3$ ($0{\cdot}50$ e Å^{-3}) is higher than in $NaNO_3$ ($0{\cdot}3$ e Å^{-3}). This depends on the contribution of the spherical parts at this point, which is larger for the N atom than for the C atom. Comparing the absolute electron density in Fig. 4 with the corresponding one of $NaNO_3$ (Göttlicher & Knöchel, 1980), we find a lower density along the *c* axis and the *xy* diagonal for the C atom in the CO_3 group. The integral $4\pi\int r^2\rho(r)dr$ with $\rho(r)$ along the *c* axis gives 5·4 e. This value is nearly the same as we get for the C atom in diamond taking the electron density $\rho(r)$ opposite the C–C bonds. In the NO_3 ion the lone pairs in the *z* direction and the overlapping of the electron made the integration difficult. In the paper of Göttlicher & Knöchel (1980), a value of 7·1 e Å^{-3} is given.

The environment of the Mg atom is drawn in Fig. 5 which corresponds to a section of the absolute densities through the equatorial plane of an MgO_6 octahedron. Two important features are to be discussed. The first is that up to 0·2 e Å^{-3} no overlap is observed between the electrons of the Mg and O atoms. The highest value of ρ between them is 0·18 e Å^{-3} and it is far from being considered as a significant covalent interaction. In addition, the integral $4\pi\int r^2\rho(r)\,dr$ with $\rho(r)$ along the *c* axis and along the diagonal of the upper square of Fig. 5 gives values of 10·4 (1) and 9·8 (1) e

respectively (mean value 10·1 e). The same value has been obtained for the Mg atom in MgF_2 (Niederauer & Göttlicher, 1970), in contrast with the 10·97 (3) e assigned to the Mg atom in dolomite, $CaMg(CO_3)_2$ (Effenberger, Kirfel & Will, 1983). We assume a quite ionic character to the Mg–O bond. The existence of a fully ionic bond in MgO has also been proposed from theoretical calculations (Causa, Dovesi, Pisani & Roetti, 1986).

The second feature refers to the electron bridge (M_O) of $\rho = 0{\cdot}24$ e Å^{-3} observed between O atoms (see lower part of Fig. 5) belonging to two different CO_3 groups. This maximum is repeated six times by the $\bar{3}$ site symmetry of the Mg atom, so forming a sectional ring cloud around it parallel to the *xy* plane. A similar electron bridge of 0·18 e Å^{-3} was also observed between neighbouring F^- anions in MgF_2 (Niederauer & Göttlicher, 1970). If we consider them as the result of a weak overlap of the lone pairs of the six O atoms surrounding the Mg atoms, we can explain (see Fig. 5) why they are located between O and O′ and not between O and O″.

Opposite a CO bond, overlapping of the lone-pair clouds is not observed. On O″ the angle between the CO bond and the line from O″ to the region where overlapping is expected is about 160° while all the other corresponding angles are between 85 and 125°. The distance between O atoms with overlapping is a little larger (3·02 Å between O and O′ and 2·93 Å between O and O″). We assume that the contact of the lone-pair clouds leads to a repulsive force between the O atoms. In $NaNO_3$, with lower charge in the cation, the O–O distances are larger (3·4 Å) and overlapping of the electron clouds is not observed.

It is desirable that further studies involving other experimental techniques confirm the existence of such O–O interactions.

We are indebted to the Deutsche Forschungsgemeinschaft and to the German and Spanish Governments for their financial support.

References

BURTON, B. & KIKUCHI, R. (1984). *Am. Mineral.* **69**, 165–175.

CAUSA, M., DOVESI, R., PISANI, C. & ROETTI, C. (1986). *Acta Cryst.* B**42**, 247–253.

EFFENBERGER, H., KIRFEL, A. & WILL, G. (1983). *Tschermaks Mineral. Petrogr. Mitt.* **31**, 151–164.

EFFENBERGER, H., MEREITER, K. & ZEMANN, J. (1981). *Z. Kristallogr.* **156**, 233–243.

GÖTTLICHER, S. (1968). *Acta Cryst.* B**24**, 122–129.

GÖTTLICHER, S. & KIESELBACH, B. (1976). *Acta Cryst.* A**32**, 185–192.

GÖTTLICHER, S. & KNÖCHEL, C. D. (1980). *Acta Cryst.* B**36**, 1271–1277.

HUMBERT, P. & PLIQUE, F. (1972). *C. R. Acad. Sci. Ser. B*, **275**, 391–394.

International Tables for X-ray Crystallography (1974). Vol. IV. Birmingham: Kynoch Press. (Present distributor Kluwer Academic Publishers, Dordrecht.)

MARKGRAF, S. A. & REDER, R. J. (1985). *Am. Mineral.* **70**, 590–600.

NIEDERAUER, K. & GÖTTLICHER, S. (1970). *Z. Angew. Phys.* **29**, 16–21.

OH, K. D., MORIKAWA, H., IWAI, S. & AOKI, H. (1973). *Am. Mineral.* **58**, 1029–1033.

PANKE, D. & WÖLFEL, E. (1969). *Z. Kristallogr.* **129**, 9–28.

PAULING, L. (1931). *J. Am. Chem. Soc.* **53**, 1367–1402.

PETERSON, R. G., ROSS, F. K., GIBBS, G. V., CHIARI, G., GUPTA, A. & TOSSELL, J. A. (1979). *Trans. Am. Geophys. Union*, **60**, 415.

SCHÄFER, C., MATOSI, F. & ADERHOLD, H. (1930). *Z. Phys.* **65**, 289–318.

VIDAL-VALAT, G., VIDAL, J. P. & KURKI-SUONIO, K. (1978). *Acta Cryst.* A**34**, 594–602.

WASER, J. (1955). *Acta Cryst.* **8**, 731.

ZACHARIASEN, W. H. (1967). *Acta Cryst.* **23**, 558–564.

ZEMANN, J. (1981). *Fortschr. Mineral.* **59**, 95–116.

ZOBETZ, E. (1982). *Z. Kristallogr.* **160**, 81–92.

Acta Cryst. (1988). B**44**, 367–373

Rietveld Profile Analysis of Calcined $AlPO_4$-11 Using Pulsed Neutron Powder Diffraction

BY JAMES W. RICHARDSON JR,* JOSEPH J. PLUTH AND JOSEPH V. SMITH

Department of Geophysical Sciences and Materials Research Laboratory, The University of Chicago, Chicago, Illinois 60637, *USA*

(*Received* 18 *August* 1987; *accepted* 15 *March* 1988)

Abstract

Aluminium phosphate, $AlPO_4$, $M_r = 121{\cdot}95$, orthorhombic, *Icmm* (disordered Al,P), *Icm*2 (ordered Al,P), $a = 13{\cdot}5333$ (8), $b = 18{\cdot}4845$ (10), $c = 8{\cdot}3703$ (4) Å, $V = 2094$ Å^3, $Z = 20$, $D_x = 1{\cdot}93$ g cm^{-3}, $T \simeq 295$ K, $R_{wp} = 0{\cdot}031$, $R_F^2 = 0{\cdot}109$ (*Icmm*) and $R_{wp} = 0{\cdot}027$, $R_F^2 = 0{\cdot}058$ (*Icm*2) for 1017 independent reflections. Sample calcined at 873 K and dehydrated at 573 K. Time-of-flight neutron powder diffraction data were

* Also Pulsed Neutron Source Division, Argonne National Laboratory, Argonne, Illinois 60439, USA.

0108-7681/88/040367-07$03.00